International Journal of Heat and Mass Transfer 53 (2010) 5722–5732

Contents lists available at ScienceDirect

International Journal of Heat and Mass Transfer

journal homepage: www.elsevier.com/locate/ijhmt

Modeling of the transport phenomena in GMAW using argon–helium mixtures. Part II – The metal

Z.H. Rao [a,b], J. Hu [c], S.M. Liao [a], H.L. Tsai [b,*]

[a] School of Energy Science and Engineering, Central South University, Changsha 410083, China
[b] Department of Mechanical and Aerospace Engineering, Missouri University of Science and Technology, Rolla, MO 65409, USA
[c] Department of Mechanical Engineering, University of Bridgeport, Bridgeport, CT 06604, USA

ARTICLE INFO

Article history:
Received 12 February 2010
Received in revised form 31 July 2010
Accepted 31 July 2010
Available online 16 September 2010

Keywords:
GMAW
Shielding gas
Plasma arc
Metal transfer

ABSTRACT

In this Part II, the effects of shielding gas compositions on transport phenomena in the metal are reported which include the transient processes of electrode melting; droplet formation, detachment, transfer and impingement onto the workpiece; weld pool dynamics and weld bead formation. It was found from the present study that electromagnetic force, which is affected by shielding gas compositions, plays the most significant role in determining the behaviors of metal transfer. For the same welding power input, the increase of helium content in the mixture leads to the formation of larger droplets and the decrease of droplet detachment frequency. The predicted phenomena on metal transfer are consistent with the reported experimental observations. Detailed discussions about the reasons causing the very interesting and unusual transport phenomena in the metal are given.

1. Introduction

A unified model and the numerical schemes capable of simulating the transport phenomena in the GMAW process have been applied in Part I [1]. The different structures and characteristics of arc plasma caused by different shielding gas compositions, including pure argon and argon–helium mixtures with various mixing ratios, have been reported. In this Part II, we present the effects of shielding gas compositions on the transient transport phenomena in the metal including the electrode melting; droplet formation, detachment, transfer and impingement onto the workpiece; weld pool dynamics and weld bead profile.

During the GMA welding process, the tip of the electrode is melted, caused by Joule heating and the heat transferred from the surrounding hot plasma, and a droplet is gradually formed. At a certain size, the droplet is detached from the electrode under the combined action of different forces including the gravity, electromagnetic force, and surface tension. The detached droplet is transferred toward the workpiece by gravity and drag force exerted by the high-speed plasma flow. The droplet carrying thermal energy impinges onto the workpiece which, along with the hot plasma and Joule heating, heats and melts the workpiece. At the same time, the mass of the droplet mixes with the workpiece to become a weld pool. The aforementioned process repeats until the welding current is turned off, the weld pool solidifies and a weld bead is formed. The GMA welding process is affected by welding voltage, current, arc length, electrode diameter and feed speed, and shielding gas [2]. Among them, the shielding gas plays a significant role by affecting the plasma generation, the forces acting on the droplet, and the arc heat flux onto the metal. The forces directly caused by shielding gas mainly consist of the arc pressure and viscous drag force of the gas flow around the droplet. Haidar [3] studied the effect of different forces acting on the droplet by including one or more forces in his modeling. Compared the calculation results with all forces included and those with each individual force being set to zero, he suggested that the forces acting on the droplet determine the metal flow in the droplet and hence, the shape, size and detachment frequency of the droplet.

In GMAW, metal is transferred from the electrode tip to the workpiece by three basic modes: the short-circuit transfer, globular transfer, or spray transfer. Globular mode involves a droplet with a diameter larger than the diameter of the electrode and a transfer rate of a few droplets per second. Above the transition current, the metal transfer changes to spray mode that is characterized by tiny droplets and an extremely high detachment frequency. The shielding gas composition affects the metal transfer mode in GMAW [4]. In pure argon shielding gas, there is a sharp transition in the droplet size and detachment frequency when the metal transfer changes from globular to spray mode [4–6]. However, for helium-rich arc welding, Rhee and Kannatey-Asibu [7] observed that metal transfer normally occurs in globular mode at any usable current level, and the droplet frequency is much smaller than that for argon. Rhee and Kannatey-Asibu [7] and

* Corresponding author. Tel.: +1 573 341 4945; fax: +1 573 341 4607.
E-mail address: tsai@mst.edu (H.L. Tsai).

0017-9310/$ - see front matter © 2010 Elsevier Ltd. All rights reserved.
doi:10.1016/j.ijheatmasstransfer.2010.08.010

Nemchinsky [8] attributed the absence of spray mode in helium-rich shielding gas to the arc contraction, which was generally regarded as being caused by high ionization potentials.

Although the information obtained through experimental observations is very useful, it is not sufficient for revealing underlying mechanisms due to the complexity of the welding process which involves high-temperature plasma and non-transparent metal. Mathematical modeling provides a convenient way to understand the physical phenomena observed in the welding process. So far, numerous models have been developed to study droplet formation [3,9–15], weld pool dynamics [16–20], and arc plasma and its influence on metal transfer [3,11–15] in GMAW. Haidar and Lowke [3,11–13] developed a model combining the arc plasma, the electrode and the workpiece to simulate the formation of droplets for the mild steel electrode in GMAW. But in their study, the droplets are neglected from the calculation after their detachment from the electrode. Fan and Kovacevic [14] predicted the globular transfer of droplets through the arc column, but in their model the arc plasma flow could not push the detached droplets downward and an empirical formulation was used to calculate the plasma drag force. Recently, Hu and Tsai [21] developed a real unified model to simulate the transport phenomena occurring during the GMAW process, including an interactive coupling between arc plasma; droplet formation, detachment and impingement onto the weld pool; and dynamics of weld pool.

In all aforementioned modeling, only pure argon was used and the influence of shielding gas compositions was not considered. Very few models [8,22,23] have been proposed to study the effect of shielding gas, especially helium or argon–helium mixtures, on the metal transfer in GMAW. Nemchinsky [8] developed a simple steady model to study the influence of different plasma gases on metal transfer. Jönsson et al. [22] discussed the metal transfer behaviors using their predicted arc parameters in argon and helium, but their model could not directly predict the phenomena of metal transfer. Haidar and Lowke [23] numerically studied the effect of carbon dioxide in shielding gas on droplet formation in GMAW. However, in their model, the droplet was ignored immediately after it was detached from the electrode tip. The weld pool dynamics was also neglected and the workpiece was treated as a flat plate in these models [22,23]. In reality, the surface of the workpiece is highly deformable and the profile of the electrode changes rapidly, which significantly influence the transport phenomena in plasma arc and metal.

From the above review, apparently the effect of shielding gas on the transport phenomena in the metal during the GMA welding process has not yet been studied and well understood. In this paper, we focus on the electrode melting; the droplet formation, detachment, transfer and impingement onto the workpiece; the weld pool dynamics and solidified bead profile in different shielding gases. The shielding gas considered in this study includes pure argon and argon–helium mixtures with various molar argon contents (75% Ar, 50% Ar, and 25% Ar). The mathematical model was presented in the first paper [1].

2. Results and discussion

The welding conditions and other parameters used in the calculations are listed in Part I [1]. In this study, a constant electric power ($uw \times I = 3500$ W) is applied and the electrode is mild steel with 1.6 mm diameter. The shielding gas varies from pure argon to argon–helium mixtures with various molar argon contents (75% Ar, 50% Ar, and 25% Ar). For each of the four shielding gases, tremendous results on the transient transport phenomena, including the distributions of temperature, velocity, current, and electromagnetic force in the metal (electrode, droplet and workpiece), the shape and location of the droplet and the weld bead shape as a function of time are all obtained. However, in the following, only the results for a typical case with 75% Ar shielding gas are presented in Figs. 1 and 2 to illustrate the general behaviors of heat transfer and fluid flow in the metal. The effects of shielding gas compositions on the aforementioned transport phenomena are given in Figs. 3–8.

2.1. Heat transfer and fluid flow in the metal

Fig. 1 shows the sequences of electrode melting; droplet formation, detachment, transfer and impingement onto the workpiece; weld pool formation; and the temperature distribution in the metal, from $t = 30$ ms to $t = 450$ ms for 75% Ar. The corresponding velocity distribution in the metal is given in Fig. 2. In order to effectively illustrate the welding phenomena of interest, the time intervals between subfigures are not equal. As shown in Fig. 1, the solid electrode tip is melted by the heat flux from the surrounding high temperature arc, and the molten metal at the tip grows and forms a droplet under the influence of surface tension. At about $t = 170$ ms, necking between the droplet and the solid electrode starts and soon thereafter the droplet is detached from the electrode. During this process, hot fluid in the droplet near its surface moves upward, turns inward near the droplet–electrode interface, and then flows downward along the center axis of the droplet, Fig. 2. There are two vortexes (in the r–z plane) in the droplet and the higher fluid temperature near its surface tends to mix with the lower molten metal temperature from the electrode which results in a more uniform temperature in the droplet. The velocity in the droplet increases as the droplet size increases and a significant inward flow appears near the neck due to the pinching effect. The droplet is detached at about $t = 176$ ms, accelerated downward, and impinges onto the workpiece at about 196 ms. At the balance of gravity, arc pressure, plasma shear stress, surface tension and electromagnetic force, the shape of the falling droplet keeps slightly changing during its transfer through the arc. The falling droplet is continually heated when it is in the flight through the arc plasma and the aforementioned mixing also continues. As a result, it is seen in Fig. 1 at $t = 192$ ms before the droplet hits the workpiece, its temperatures are higher and more uniform as compared to when the droplet was just detached from the electrode. The temperature increase in the droplet is mainly caused by the surrounding high-temperature plasma arc. As discussed in Part I [1], the electric current can flow through the falling droplet just after detachment, but the electrical conductivity is very high and thus the Joule heating can be neglected. During the process of droplet transfer through the arc plasma, the workpiece continues to be heated up by the arc plasma.

At $t = 196$ ms, the detached droplet hits the solid workpiece with a rather high axial velocity of about 50 cm/s, Fig. 2. Then, the droplet quickly spreads outward along the workpiece surface. As the droplet contains a large amount of thermal energy, it provides additional energy to heat and melt the workpiece. Hence, the mass, momentum, and thermal energy carried by the droplet are mixed and merged into the workpiece. A weld pool is then gradually formed as more droplets impinge onto the workpiece. Due to the downward momentum of the droplet, a crater is formed at the weld pool center, $t = 202$ ms. However, under the actions of surface tension and hydrostatic force, the crater is quickly being flattened and the fluid at the center continues to go upward, as shown at $t = 212$ ms. Then, the raised surface at the weld pool center is pushed down by the surface tension, arc pressure force, and hydrostatic force at $t = 236$ ms. The weld pool up-and-down dynamics are similar to those described in Ref. [18]. The equilibrium of the weld pool is achieved and the shape of the weld pool remains nearly unchanged at $t = 296$ ms until a new droplet

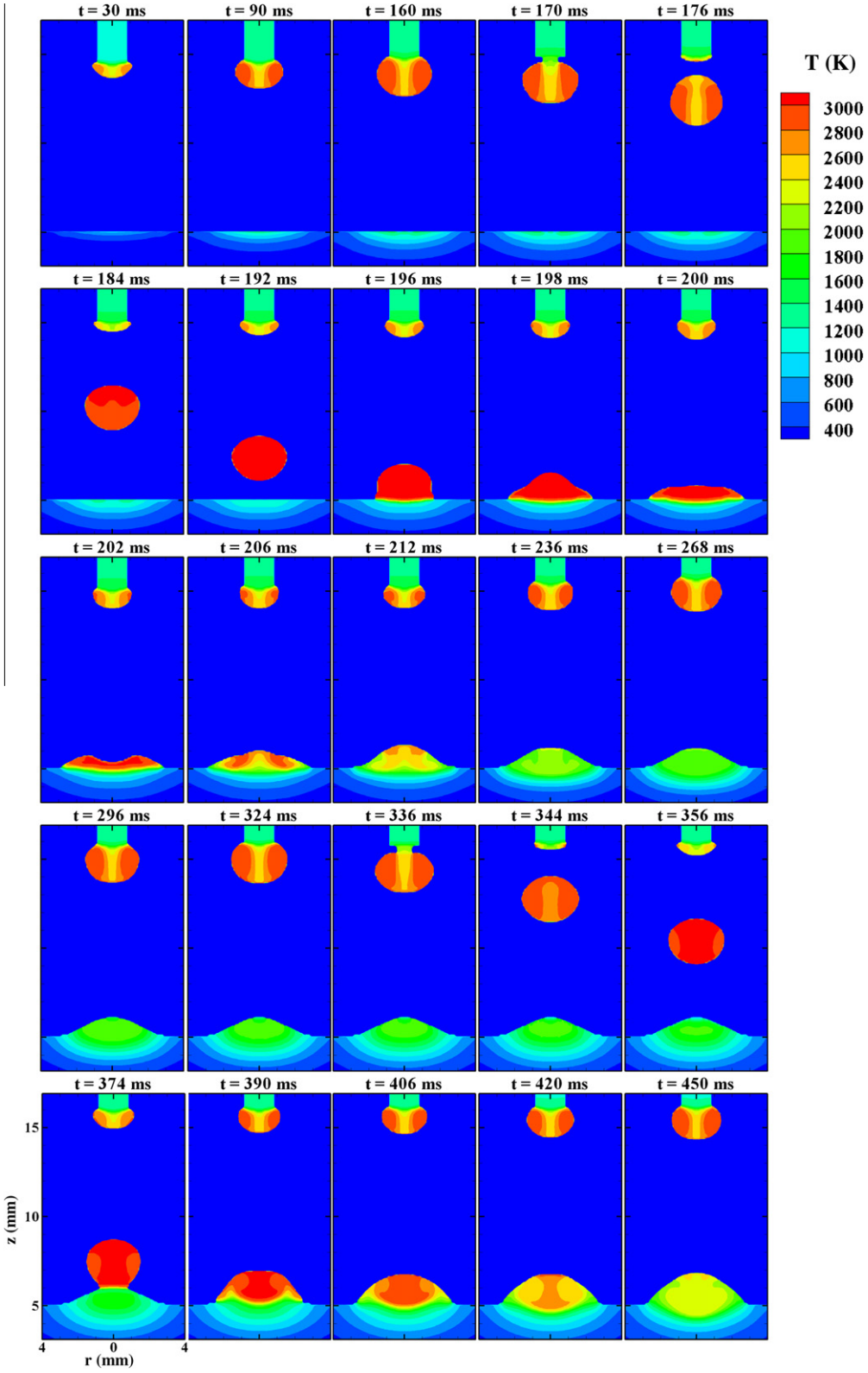

Fig. 1. A sequence of electrode melting; droplet formation, detachment, transfer, and impingement onto the weld pool; weld bead formation; temperature distribution in the metal for 75% Ar.

impinges. At the same time, the weld pool loses heat to the surrounding cold metals by heat conduction and, hence, the temperature and velocity in the weld pool decrease continuously. Before the second droplet impinges onto the weld pool, the weld pool is almost solidified, $t = 356$ ms, Fig. 2. As soon as the first droplet was detached from the electrode, the second droplet starts to form, undergoing the same aforementioned procedure as the first droplet, and impinges onto the nearly solidified weld pool at $t = 374$ ms. After the second droplet deposits onto the weld pool, the weld pool becomes larger and the penetration increases. The

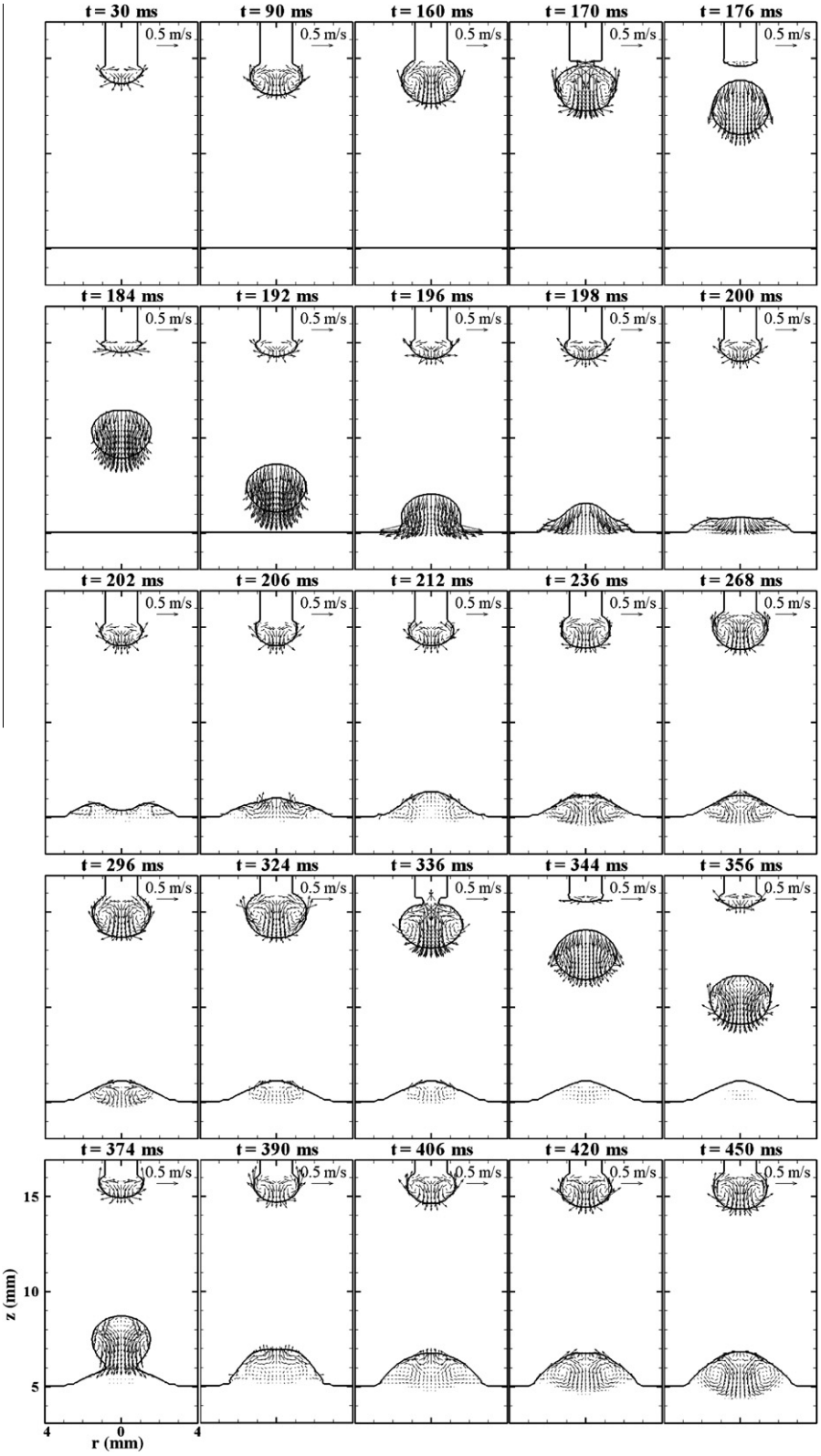

Fig. 2. The corresponding velocity distribution for the case as shown in Fig. 1.

aforementioned cycle including the electrode melting, droplet generation, detachment, transfer, and impingement onto the weld pool repeats until the desired weld bead size or welding time is achieved.

2.2. Effects of shielding gas compositions on the metal

Figs. 3–5 present, respectively, the temperature, velocity and electromagnetic force distributions in the metal for different

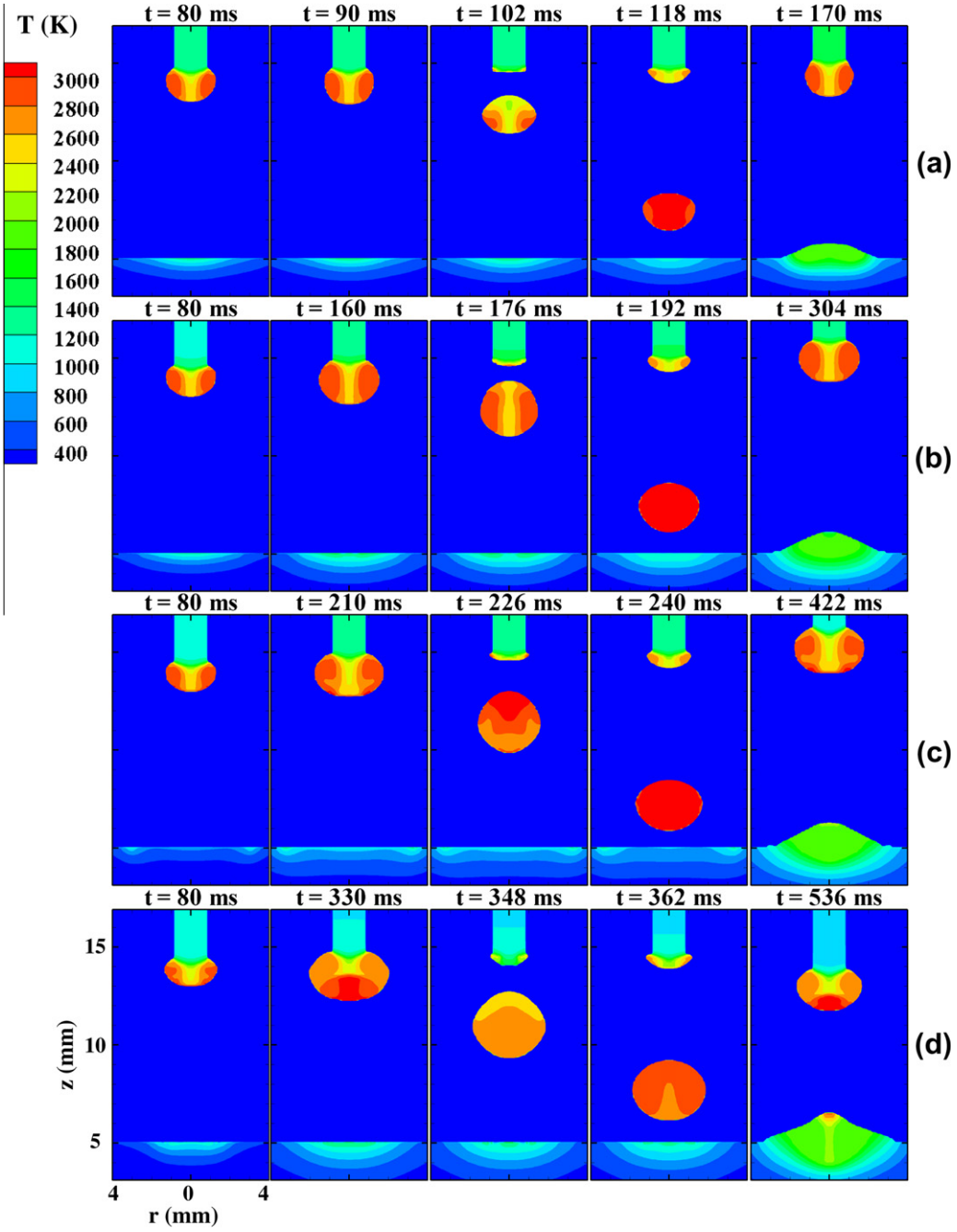

Fig. 3. Comparison between different shielding gases on the temperature distribution and the first droplet formation, detachment, transfer, and impingement onto the weld pool: (a) pure Ar, (b) 75% Ar, (c) 50% Ar and (d) 25% Ar.

shielding gases during the sequence of the first droplet generation, detachment, transfer, and impingement onto the workpiece. As shown in Fig. 3, the process of droplet formation and transfer for pure Ar, 50% Ar and 25% Ar are generally similar to the case of 75% Ar which was described before. Note in order to facilitate the following discussion, the instant of each selected subfigure and the time lag between two subfigures for each gas or between two different gases are not the same. When helium is added to argon gas, the droplet diameter increases and is larger than the electrode diameter and, hence, the metal transfer mode remains in the globular regime. However, the droplet size and droplet formation time increase when the helium content increases. The droplets are, respectively, detached at about $t = 100$ ms, 170 ms, 217 ms and 336 ms for pure Ar, 75% Ar, 50% Ar and 25% Ar. The results are consistent with the experimental observation [7] that the droplet frequency using argon is much higher than that for helium.

As shown in Fig. 4 at $t = 80$ ms, the droplet volume is smaller in high helium arcs ((c) 50% Ar and (d) 25% Ar) which indicates the electrode melting rate decreases with the increase of helium content for the same welding power input. At $t = 80$ ms, the welding currents are 230 Å, 210 Å, 184 Å, and 161 Å, respectively, for pure Ar, 75% Ar, 50% Ar, and 25% Ar. As a result of the lower current level and higher ionization potential of helium, the temperatures in the arc and in the solid electrode are lower for the cases with higher helium content. Therefore, with the increasing helium content, both the arc heating and Joule heating to the electrode decrease with the result of a reduced melting rate of the electrode, which prolongs the droplet formation time. At $t = 80$ ms, the increase of

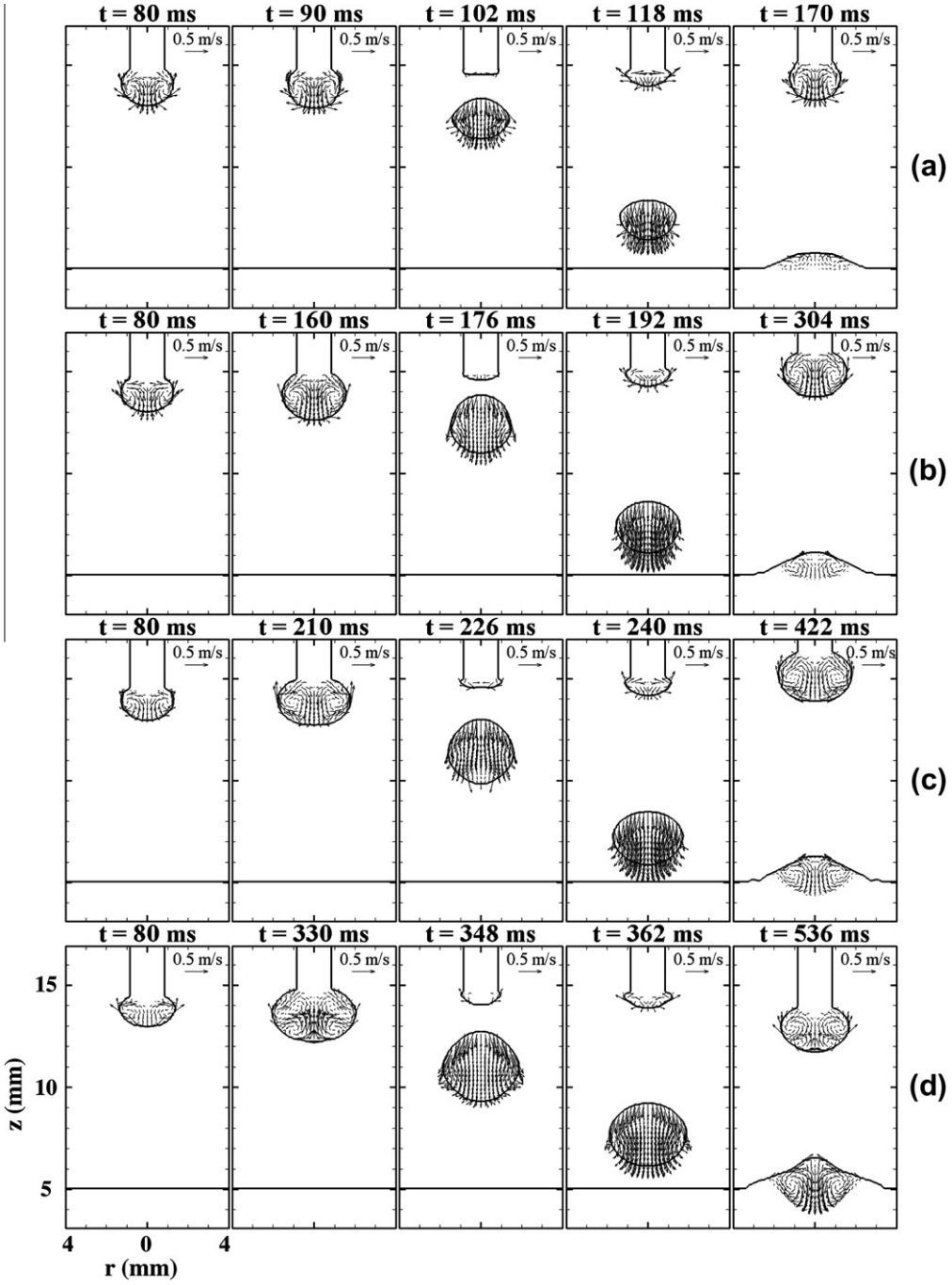

Fig. 4. The corresponding velocity distribution in the metal for the cases as shown in Fig. 3: (a) pure Ar , (b) 75% Ar, (c) 50% Ar and (d) 25% Ar.

helium content leads to smaller velocities in the droplet, Fig. 4, which also causes a less uniform temperature distribution and higher temperature gradients in the droplet, Fig. 3. The maximum temperatures found at the surface of the droplet are, respectively, 2914 K and 2963 K for pure Ar and 75% Ar, and approach the vaporization temperature of 3080 K for 50% Ar and 25% Ar. At the instants before necking (Fig. 3, $t = 90$ ms, 160 ms, 210 ms, and 330 ms for pure Ar, 75% Ar, 50% Ar and 25% Ar, respectively), the welding currents are, respectively, 230 Å, 215 Å, 190 Å, and 166 Å. In the first and second column of Fig. 3, before detachment, it is seen the shape of the droplet is more spherical in the pure argon arc and is more oblate in the high helium arc, which is consistent with the phenomena observed by Rhee and Kannatey-Asibu [7]. For pure argon, at a current less than the transition value (which is 275 Å for 1.6 mm of mild steel electrode [2]), the metal transfer mode is globular and the droplet at the tip of the electrode is a round shape, which is in agreement with the experimental results of Jones et al. [5,24,25].

In addition to the lower melting rate as discussed above, the longer droplet formation time in the high helium arc is mainly attributed to the combined effect of the forces acting on the droplet, including the electromagnetic force, surface tension, gravity, arc pressure, and plasma shear stress. Among these forces, electromagnetic force is the very important one which behaves quite differently in different shielding environments. The magnitude and direction of the electromagnetic force are determined by the

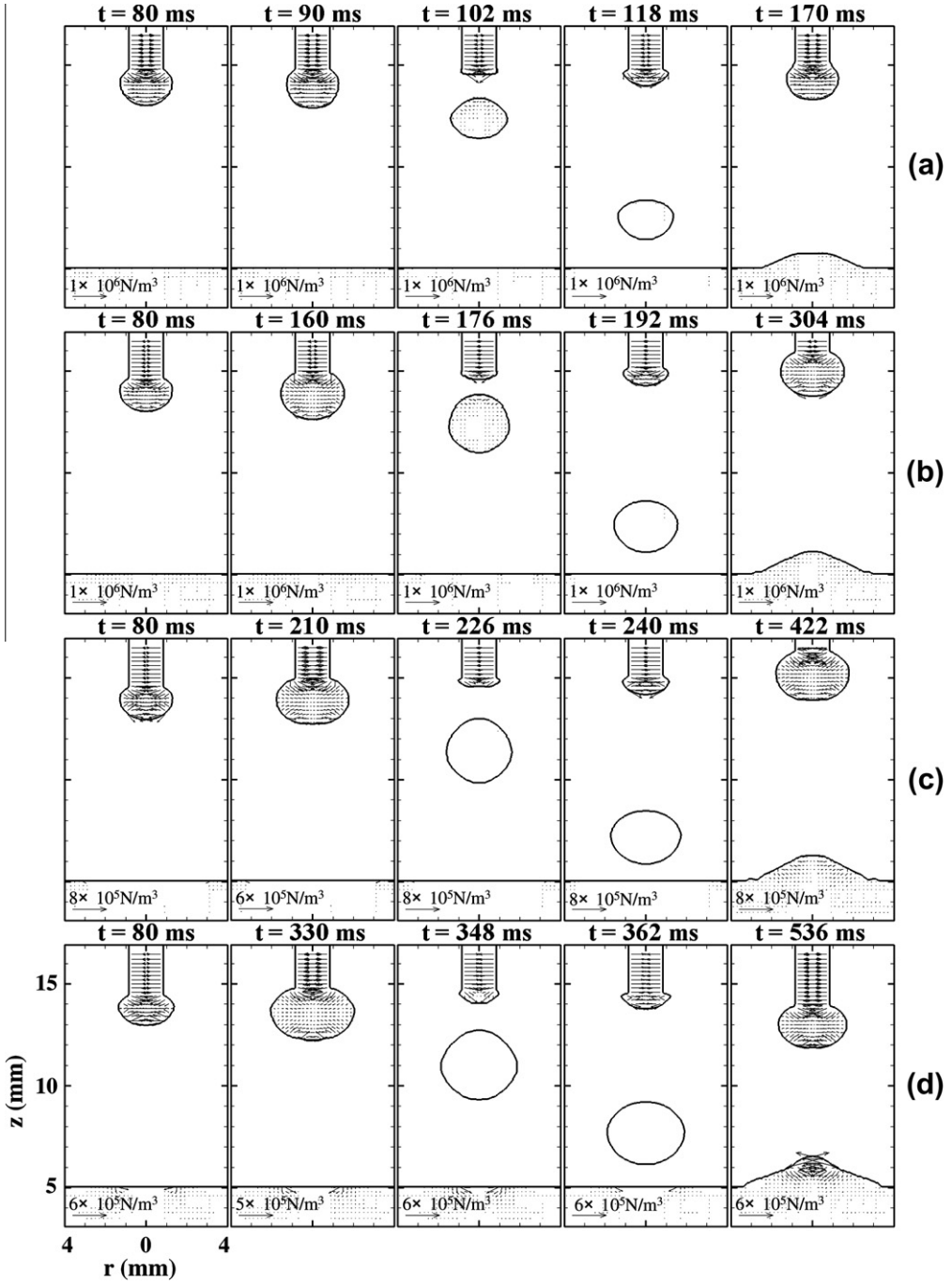

Fig. 5. The corresponding electromagnetic force distribution in the metal for the cases as shown in Fig. 3: (a) pure Ar, (b) 75% Ar, (c) 50% Ar and (d) 25% Ar.

current through the electrode. As shown in Fig. 6 of Part I [1], the current flow in the electrode is parallel to its axis, slightly diverges in the upper portion of the droplet, and then diverges in the lower portion of the droplet, and finally emerges out from the droplet. Therefore, for all cases in Fig. 5, the electromagnetic force near the neck of the electrode is downward and inward. The inward radial component of the electromagnetic force ($-J_z \times B_\theta$) has a pinch effect on the droplet and thus it is a detaching force. For pure argon, Fig. 5(a), the axial component of the electromagnetic force ($J_r \times B_\theta$) is downward and is a detaching force that pushes the liquid metal away from the electrode. As the helium content increases, there exists an upward and inward electromagnetic force near the bottom of the droplet which becomes an attaching force that sustains the droplet. The attaching effect of the electromagnetic force at the bottom becomes stronger with the increase of helium content, particularly for the case of 25% Ar. As helium increases in the shielding gas, an obvious arc contraction appears underneath the droplet (not detached yet) due to the high ionization potential of helium (first column of Fig. 6 in Part I [1]). The arc contraction causes current flows to leave the droplet from a smaller area at the bottom surface of the droplet and thus induces the inward and downward current flows in the lower part of the droplet, Fig. 6 in Part I [1], which, in turn, produces an upward and inward electromagnetic force for repelling the droplet, as shown in Fig. 5(d). The downward electromagnetic force near the top of the droplet and the upward electromagnetic force near the bottom

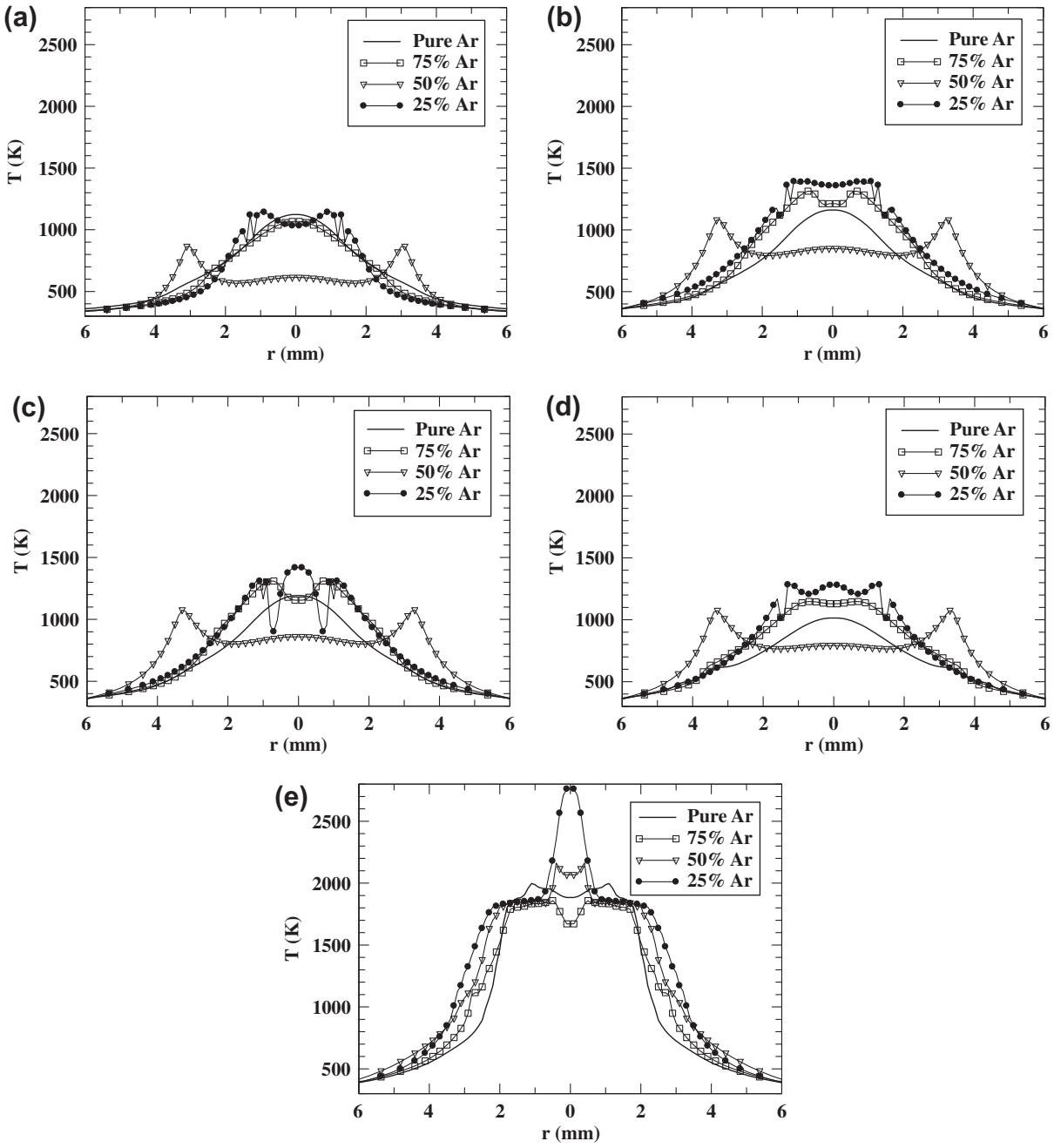

Fig. 6. The metal temperature along the workpiece surface at different instants for the cases as shown in Fig. 3: (a) the first column, (b) the second column, (c) the third column, (d) the fourth column and (e) the fifth column.

of the droplet tend to "squeeze" the droplet to become an oblate shape, for example, as shown at $t = 330$ ms for 25% Ar in Fig. 5(d). On the other hand, due to the lower current for higher helium content at the constant electric power input, the electromagnetic force decreases and, thus, produces a weaker pinch effect, which also increases the droplet formation time. Therefore, the electromagnetic force in high helium arcs leads to the formation of an oblate droplet and the increase of droplet formation time. However, as the detaching force, mainly the weight of the droplet, eventually exceeds the attaching force, the droplet is detached from the electrode.

The change of electromagnetic force in high helium arcs also strongly influences the temperature distribution and fluid flow pattern in the droplet. It is seen in Fig. 3 for 25% Ar at $t = 330$ ms and $t = 536$ ms, the lower part of the droplet has much higher temperatures than the upper part. In the corresponding subfigures in Fig. 4, the fluid at the bottom of the droplet flows upward along its axis which meets another fluid flowing downward in the upper part of the droplet. Hence, there are four vortexes in the droplet at $t = 330$ ms for 25% Ar; two are in the upper part of the droplet and the other two are in the lower part of the droplet. As the hot fluid does not mix well with the cold fluid in the droplet, the temperature is not uniform in the droplet, Fig. 3. This is in contrast to the argon-rich mixtures in which there are only two vortexes in the droplet and the mixing is better. From the third and forth column in Fig. 5, after the droplet is detached, the electromagnetic force acting on the detached droplet decreases dramatically in all cases because most of the current flows around and bypass the droplet,

especially when the droplet moves further away from the electrode, Fig. 6 of Part I. The electromagnetic force in the detached droplet almost disappears in high helium arcs.

Fig. 6 shows the metal temperature along the surface of the workpiece for all cases corresponding to Fig. 3. Before the droplet reaches the workpiece, the increase of metal temperature is primarily caused by current Joule heating and arc heat flux. For the first column in Fig. 3, for pure argon and 75% Ar, the temperature distribution along the surface of the workpiece is a Gaussian-like shape with the maximum temperature occurring at the center $r = 0$ of the workpiece. When the helium increases, at 50% Ar, the temperature distribution is M-shaped with two peaks (the peak temperatures form a ring or circle shape in an axisymmetric coordinate system) at which the current converges, Fig. 6(c) in Part I. However, near the center, the temperature is rather flat and low which is consistent with the low current density shown in Fig. 6(c) of Part I. The unusual flat temperature along the workpiece surface for 50% Ar can also be seen in Fig. 3(c). However, the range of the "high surface temperature" for 50% Ar is wider than all other cases. As the helium content further increases (25% Ar), the two peaks are "squeezed" toward the center at which the current converges, Fig. 6(d) of Part I. Compared to the case of 50% Ar, the temperatures are much higher near the center but narrower in scope for 25% Ar. As the droplet becomes larger, detached from the electrode but not yet impinges onto the workpiece, the temperature distributions along the workpiece surface, Fig. 6(b)–(d), are generally similar to those in Fig. 6(a), except for the case of 25% Ar in which the temperature fluctuates near the center of the workpiece. As shown in Fig. 6(e), when the droplet impinges onto the weld pool, the base metal is significantly heated up to above the melting point by the thermal energy carried by the droplet. The temperature profiles along the surface of the workpiece are very similar in shape and smooth for all cases except near the center of the workpiece where the temperatures fluctuate. Depending upon the size of the droplet, at the same location, the temperature increases as the helium content increases. Note the droplet impinges onto the workpiece at different times for different argon contents in Fig. 6.

Fig. 7 shows the distributions of electromagnetic force and arc flow velocity for 25% Ar at different instants. Note only a quarter of the grid nodes are used in order to increase the readability of vectors. It is seen there exist significant upward electromagnetic forces in the arc near the workpiece, Fig. 7(a). This leads to strong upward plasma flows and generates two vortexes near the workpiece, Fig. 7(b). These vortexes although weak, slow down and change the flow direction of the strong plasma flow from the electrode. When the droplet is still not detached from the electrode ($t = 330$ ms, 536 ms and 720 ms), the vortexes are limited to a relatively small region near the workpiece. However, after the droplet is detached and transfers in the middle between the electrode and the workpiece ($t = 348$ ms and 680 ms), the droplet blocks, weakens and changes the direction of plasma flow from the electrode; while the aforementioned two vortexes near the workpiece become stronger and expand to the whole region between the falling droplet and the workpiece. Hence, the falling droplet is subject to a strong upward flow which leads to high arc pressures underneath the falling droplet (as shown in Fig. 9 of Part I). Jönsson et al. [22] argued that the droplets formed in helium arcs are subject to upward forces (repelling forces) which may lead to the drift of droplets randomly in a sideway direction, causing the so-called repelled metal transfer [7,26]. The existence of a strong electromagnetic force near the workpiece and the resulting repelling force in helium arcs were also discussed elsewhere [27,28]. The aforementioned results predicted by the present model appear to support the cathode jet theory that was proposed by Maecker [28] that the cathode force is responsible for the repelled metal transfer.

The weld current is turned off at $t = 800$ ms for all cases, and then solidification begins. At this instant, the numbers of droplets deposited onto the workpiece are, respectively, 7, 4, 3, 2 for pure Ar, 75% Ar, 50% Ar and 25% Ar. The final shapes of the weld beads are shown in Fig. 8. A weld bead profile is usually described by the penetration area/volume (the area/volume of the base material

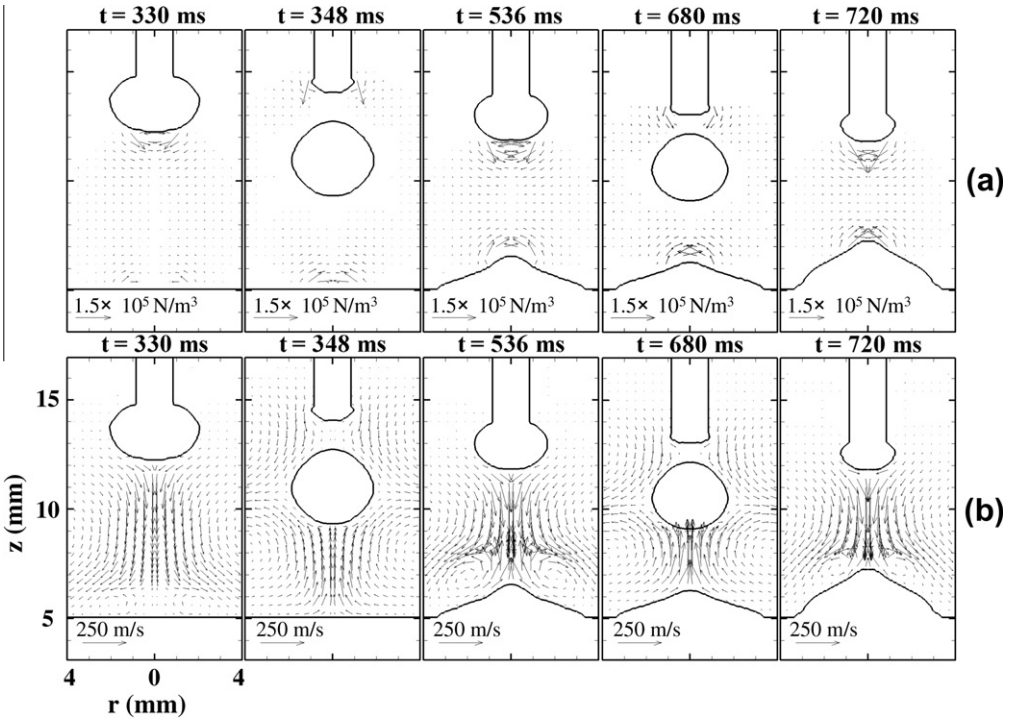

Fig. 7. The distributions of (a) electromagnetic force and (b) flow velocity in the arc of 25% Ar at different instants.

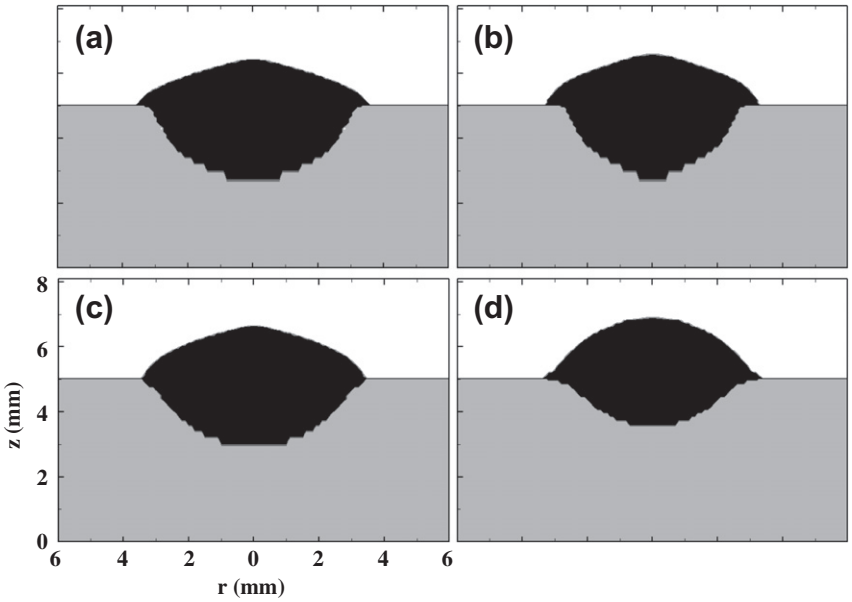

Fig. 8. The solidified weld bead shapes: (a) pure Ar, (b) 75% Ar, (c) 50% Ar and (d) 25% Ar.

that was melted) and the reinforcement area/volume (the area/volume of metal above the initial surface of the workpiece), as well as the bead width, bead height and penetration depth. As the wire feed speeds are the same for all cases, theoretically the reinforcement area/volume should be the same (neglecting possible metal evaporation). However, as the electrode may be partially melted and a whole droplet has not yet been completely formed and detached at t = 800 ms, the reinforcement area/volume will not be exactly the same among all cases. From Fig. 8, it appears the area/volume of the weld bead and the penetration depth decrease as the helium content increases, particularly for the case of 25% Ar. Hence, for the same welding energy input, the welding efficiency and, perhaps, weld bead quality, are better for shielding gases with higher argon content.

3. Conclusions

Using a unified gas metal arc welding model, the influences of shielding gas compositions on the transient transport phenomena in the metal, including electrode, droplet and workpiece were studied. The phenomena of fluid flow and heat transfer in the metal using various shielding gases were compared. In pure argon shielding, the axial component of the electromagnetic force acting on the droplet is a detaching force that contributes to the separation of the droplet from the electrode. In high helium arcs, the axial electromagnetic force at the bottom of the droplet becomes an attaching force, due to arc contraction, which sustains the droplet at the electrode tip and causes the droplet to be less spherical. Hence, the increase of helium content in the shielding gas increases droplet size and droplet formation time, and decreases droplet detachment frequency for welding at a constant welding energy input. A significant upward electromagnetic force near the workpiece is also predicted in high helium arcs, caused by arc contraction, which is consistent with the cathode jet theory that cathode force is responsible for the repelled metal transfer. The Gaussian-like distribution of temperature along the workpiece is found for pure argon shielding gas before droplet impingement. As helium content increases, however, the temperature distributions along the workpiece surface exhibit various extents of distortions and fluctuations, which are combined results of the arc contraction and current convergence at the workpiece.

References

[1] Z.H. Rao, J. Hu, S.M. Liao, H.L. Tsai, Modeling of the transport phenomena in GMAW using argon–helium mixtures. Part I - The arc, Int. J. Heat Mass Transfer 53 (2010) 5707–5721.
[2] D.B. Holliday, Gas–Metal Arc Welding, in: D.L. Olson, T.A. Siewert, S. Liu, G.R. Edwards (Eds.), ASM Handbook, vol. 6: Welding, Brazing, and Soldering, American Society for Metals, Metals Park, OH, 1993, pp. 180-185.
[3] J. Haidar, An analysis of the formation of metal droplets in arc welding, J. Phys. D: Appl. Phys. 31 (1998) 1233–1244.
[4] K.A. Lyttle, shielding gas for welding, in: D.L. Olson, T.A. Siewert, S. Liu, G.R. Edwards (Eds.), ASM Handbook, vol. 6: Welding, Brazing, and Soldering, American Society for Metals, Metals Park, OH, 1993, pp. 64-69.
[5] L.A. Jones, T.W. Eagar, J.H. Lang, Images of steel electrode in Ar-2%O_2 shielding during constant current gas metal arc welding, Weld. J. 77 (1998) 135s–141s.
[6] Q. Lin, X. Li, S.W. Simpson, Metal transfer measurements in gas metal arc welding, J. Phys. D: Appl. Phys. 34 (2001) 347–353.
[7] S. Rhee, E. Kannatey-Asibu, Observation of metal transfer during gas metal arc welding, Weld. J. 71 (1992) 381s–386s.
[8] V.A. Nemchinsky, The effect of the type of plasma gas on current contraction at the molten tip of an arc electrode, J. Phys. D: Appl. Phys. 29 (1996) 1202–1208.
[9] S.K. Choi, C.D. Yoo, Y.S. Kim, The dynamic analysis of metal transfer in pulsed current gas metal arc welding, J. Phys. D: Appl. Phys. 31 (1998) 207–215.
[10] F. Wang, W.K. Hou, S.J. Hu, E. Kannatey-Asibu, W.W. Schultz, P.C. Wang, Modelling and analysis of metal transfer in gas metal arc welding, J. Phys. D: Appl. Phys. 36 (2003) 1143–1152.
[11] J. Haidar, J.J. Lowke, Predictions of metal droplet formation in arc welding, J. Appl. Phys. D: Appl. Phys. 29 (1996) 2951–2960.
[12] J. Haidar, Prediction of metal droplet formation in gas metal arc welding II, J. Appl. Phys. 84 (1998) 3530–3540.
[13] J. Haidar, An analysis of heat transfer and fume production in gas metal arc welding. III, J. Appl. Phys. 85 (1999) 3448–3459.
[14] H.G. Fan, R. Kovacevic, A unified model of transport phenomena in gas metal arc welding including electrode, arc plasma and molten pool, J. Phys. D: Appl. Phys. 37 (2004) 2531–2544.
[15] H.G. Fan, R. Kovacevic, Droplet formation, detachment, and impingement on the molten pool in gas metal arc welding, Metall. Trans. 30B (1999) 791–801.
[16] Y. Wang, H.L. Tsai, Impingement of filler droplets and weld pool dynamics during gas metal arc welding process, Int. J. Heat Mass Transfer 44 (2001) 2067–2080.
[17] Y. Wang, Q. Shi, H.L. Tsai, Modeling of the effects of surface-active elements on flow patterns and weld penetration, Metall. Trans. 32B (2001) 145–161.
[18] Y. Wang, H.L. Tsai, Effects of surface active elements on weld pool fluid flow and weld penetration in gas metal arc welding, Metall. Trans. 32B (2001) 501–515.

[19] H.G. Fan, R. Kovacevic, Dynamic analysis of globular metal transfer in gas metal arc welding – a comparison of numerical and experimental results, J. Phys. D: Appl. Phys. 31 (1998) 2929–2941.
[20] Z. Cao, Z. Yang, X.L. Chen, Three-dimensional simulation of transient GMA weld pool with free surface, Weld. J. 82 (2004) 169s–176s.
[21] J. Hu, H.L. Tsai, Heat and mass transfer in gas metal arc welding, Part II: The metal, Int. J. Heat Mass Transfer 50 (2007) 808–820.
[22] P.G. Jönsson, T.W. Eagar, J. Szekely, Heat and metal transfer in gas metal arc welding using argon and helium, Metall. Trans. 26B (1995) 383–395.
[23] J. Haidar, J.J. Lowke, Effect of CO_2 shielding gas on metal droplet formation in arc welding, IEEE Trans. Plasma Sci. 25 (1997) 931–936.
[24] L.A. Jones, T.W. Eagar, J.H. Lang, Magnetic forces acting on molten drops in gas metal arc welding, J. Phys. D: Appl. Phys. 31 (1998) 93–106.
[25] L.A. Jones, T.W. Eagar, J.H. Lang, A dynamic model of drops detaching from a gas metal arc welding electrode, J. Phys. D: Appl. Phys. 31 (1998) 107–123.
[26] Y.S. Kim, D.M. McEligot, T.W. Eagar, Analysis of electrode heat transfer in gas metal arc welding, Weld. J. 70 (1991) 20s–30s.
[27] T.B. Hazlett, G.M. Gordon, Studies of welding arcs using various atmospheres and power supplies, Weld. J. 36 (1957) 382s–386s.
[28] H. Maecker, Z. Phys. 141 (1955) 198–216.